The Native State Conformational Ensemble of the SH3 Domain from α-Spectrin†

Mourad Sadqi, Salvador Casares, María A. Abril, Obdulio López-Mayorga, and Francisco Conejero-Lara*

Department of Physical Chemistry and Institute of Biotechnology, University of Granada, 18071 Granada, Spain

Ernesto Freire*

Department of Biology and Biocalorimetry Center, The Johns Hopkins University, Baltimore, Maryland 21218

Received February 22, 1999; Revised Manuscript Received May 5, 1999

ABSTRACT: The folding/unfolding equilibrium of the α-spectrin SH3 domain has been measured by NMR-detected hydrogen/deuterium exchange and by differential scanning calorimetry. Protection factors against exchange have been obtained under native conditions for more than half of the residues in the domain. Most protected residues are located at the β-strands, the short 3_{10} helix, and part of the long RT loop, whereas the loops connecting secondary structure elements show no measurable protection. Apparent stability constants per residue and their corresponding Gibbs energies have been calculated from the exchange experiments. The most stable region of the SH3 domain is defined by the central portions of the β-strands. The peptide binding region, on the other hand, is composed of a highly stable region (residues 53−57) and a highly unstable region, the loop between residues 34−41 (n-Src loop). All residues in the domain have apparent Gibbs energies lower than the global unfolding Gibbs energy measured by differential scanning calorimetry, indicating that under our experimental conditions the amide exchange of all residues in the SH3 domain occurs primarily via local unfolding reactions. A structure-based thermodynamic analysis has allowed us to predict correctly the thermodynamics of the global unfolding of the domain and to define the ensemble of conformational states that quantitatively accounts for the observed pattern of hydrogen exchange protection. These results demonstrate that under native conditions the SH3 domain needs to be considered as an ensemble of conformations and that the hydrogen exchange data obtained under those conditions cannot be interpreted by a two-state equilibrium. The observation that specific regions of a protein are able to undergo independent local folding/unfolding reactions indicates that under native conditions the scale of cooperative interactions is regional rather than global.

For many years, our view of the folding equilibrium in proteins has been distorted by the so-called two-state model, in which proteins are assumed to be in equilibrium between two discrete states, the native and unfolded states. Today, we know that the two-state view is misleading and that the behavior observed under transition conditions cannot be extrapolated to native conditions. In particular, the heterogeneity in the pattern of hydrogen exchange protection measured by NMR for many proteins has demonstrated the existence of multiple conformations under equilibrium conditions and cannot be rationalized in terms of the two-state model (*1*−*13*).

In hydrogen/deuterium exchange experiments performed under the so-called EX2 regime (see, for example, refs *8* and *14* and below), amide groups that are buried from the solvent in the native structure become able to undergo the exchange reaction as a result of some unfolding event or conformational change that render them exposed to the solvent. If only two states were accessible to a protein, all amide groups that are protected in the native state would exhibit the same protection factors since the same unfolding event will expose all of them to the solvent. Moreover, the Gibbs energy calculated from this event would be equal to the global Gibbs energy for global unfolding. This is not what is observed experimentally. For all proteins studied to date, the pattern of protection factors shows significant variations between residues, indicating that certain amide groups become exposed to the solvent as a result of local rather than global unfolding events (*1*−*8, 12, 13, 15*−*18*). These local unfolding events occur independently of each other and give rise to a large number of conformational states in which small regions of the protein fold and unfold in all possible combinations. Under equilibrium conditions the probabilities of those conformations are dictated by their Gibbs energies.

In this paper we have studied the conformational equilibrium of the SH3[1] domain from α-spectrin. SH3 domains are small conserved modular domains (∼60 amino acids) that mediate protein−protein interactions in cellular signaling cascades and many other important biological processes *(19*−*23)*. The structure of several SH3 domains is known at high

† Supported by grants from the DGICYT (PB96-1446) (Spain), the European Commission (PL95-0200 and PL96-2180), the National Science Foundation (MCB-9816661), and the National Institutes of Health (GM51362) (Baltimore).

* Correspondence can be addressed to either author.

[1] Abbreviations: SH3, Src homology region 3; SDS−PAGE, sodium dodecyl sulfate−polyacrylamide gel electrophoresis; COSY, scalar coupling correlated spectroscopy; DSC, differential scanning calorimetry.

10.1021/bi990413g CCC: $18.00
Published on Web 06/19/1999

resolution. In general, SH3 domains fold as compact β-barrels with five to six antiparallel β-strands. SH3 domains mediate protein−protein interactions and modulate enzyme activity by their ability to bind specific proline-rich peptides. Since SH3 domains receive and transmit information via these specific interactions, it is important to understand how the structural cooperativity is propagated through the native domain structure. The combined use of NMR-detected hydrogen−deuterium exchange and high-sensitivity differential scanning calorimetry provides a unique way of measuring residue-level and global stability parameters and, therefore, of exploring the nature of the native state conformational ensemble.

MATERIALS AND METHODS

Protein Expression and Purification. Wild-type SH3 was overexpressed from a pET3d plasmid in the *Escherichia coli* BL21 (DE3) strain. The plasmid was a kind gift from Dr. Luis Serrano (EMBL, Heidelberg). Collected cells were lysed in 5 mM sodium citrate, pH 3.5, in a French press, and the protein was recovered from the supernatant by precipitation in ammonium sulfate at 75%. Precipitated protein was solubilized in 50 mM sodium phosphate buffer and 100 mM NaCl, pH 7.0, containing 6 M urea, and dialyzed extensively against the same buffer. The protein was purified by a gel filtration step on a Hi-Load Superdex 75 column (Pharmacia), and purity was checked by SDS−PAGE electrophoresis.

Hydrogen Exchange. Exchange samples were prepared from a stock solution of α-spectrin SH3 by extensively dialyzing it against deionized water and further lyophilization. H−D exchange was initiated by rapidly dissolving the lyophilized protein in deuterated buffer (20 mM d_5-glycine for pH* 3.0 and pH* 2.5 or 20 mM d_3-acetate for pH* 4.0). The sample was filtered to remove insoluble protein, and then immediately placed in a 5 mm NMR tube and into the magnet. The final protein concentration was approximately 5 mM when dissolved in 500 μL of deuterated buffer. The pH* of samples was checked after each experiment. Values of pH* reported in D_2O solutions represent direct pH meter readings, without correction for isotope effects. The experiment dead times (i.e., time between dissolving the protein and the start of data acquisition) were between 15 and 20 min. The probe temperature was determined immediately before each experiment using a sample of 80% ethylene glycol and 20% d_6-dimethyl sulfoxide. Magnet shims were preadjusted on a sample identical to the exchange one. All NMR experiments were performed at 24.7 °C on a Brüker AMX-500 spectrometer belonging to the instrumentation center of the University of Granada. A set of 20−30 two-dimensional phase-sensitive COSY spectra were acquired during the exchange at progressively longer time intervals. Acquisition was performed using the time-proportional phase incrementation technique (TPPI) (*24*). Data sets comprised 256 × 2048 data points and the spectral width was 6024 Hz. A light presaturation of the residual water signal was done during the relaxation delay.

The program package NMRpipe (*25*) was used to process the NMR data on a Silicon Graphics O2 workstation. Prior to Fourier transformation, the 2D data matrix was multiplied by a square-sine bell window function in both dimensions and then zero-filled to 4096 × 4096 words. The NMRview package (*26*) was used for computerized cross-peak identification and analysis. The assignment of the COSY NH−C_αH cross-peaks of our spectra was readapted to our experimental conditions, taking as a reference the published assignment at pH 3.5 and 35 °C (*27*). The intensity of each NH−C_αH cross-peak was taken to be the average of the intensities (absolute values) of the four components of the COSY cross-peak and was normalized by comparison with the averaged intensity of the cross-peak C_αH−C_βH corresponding to the nonexchangeable protons of Ala55. For each residue, the normalized peak intensity was considered to be proportional to the proton occupancy of the corresponding amide group. The time assigned to each proton occupancy value was taken to be the middle of the acquisition time for each COSY spectrum, and "time zero" is the time when the protein was dissolved into deuterated buffer.

The exchange kinetics of 33−39 amide protons could be measured, depending on the conditions. A single-exponential decay function, $I = I_0 \exp(-k_{ex}t) + c$, was fitted to the normalized cross-peak intensities in order to determine their exchange rate constants, k_{ex}. I is the normalized signal intensity at time t (in seconds), I_0 is the amplitude of the exchange curve, k_{ex} is the observed hydrogen exchange rate constant, and the constant c is the peak intensity at the infinity time point. A home made program was used to calculate the sequence-specific intrinsic rate constants of exchange for each amide proton, k_{int}, at the different pH* values using the exchange data of Bai et al. (*28*) for model peptides.

Protection factors against exchange, PF, were determined as $PF = k_{int}/k_{ex}$.

Under our experimental conditions, the intrinsic exchange rate constants for all amide protons are several orders of magnitude lower than the reported refolding rate constant of α-spectrin SH3 (*20*). Accordingly, an EX2 mechanism for the amide hydrogen exchange could be assumed (*28*).

Under EX2 exchange, for a particular residue, the equilibrium between the "open" state, in which the amide proton is exchange competent, and the "closed" state, in which the amide proton is protected against exchange, is fully established and the opening equilibrium constant, K_{op}, can be obtained as follows: $K_{op} = k_{ex}/k_{int} = (PF)^{-1}$. For each residue, the free energy difference between the closed and the open states is given by

$$\Delta G = -RT \ln K_{op} = -RT \ln(1/PF) \qquad (1)$$

Calorimetry. High-sensitivity differential scanning calorimetry (DSC) was performed in deuterium oxide (D_2O) solutions using a VP-DSC microcalorimeter (Microcal) at a scan rate of 60 deg/min. Unfolding experiments were carried out in 20 mM glycine or 20 mM acetate buffers in D_2O at different values of pH* between 1.0 and 4.5. The samples were prepared by dissolving the lyophilized protein into the D_2O buffers and then filtering the solutions with a 0.2 μm Millex filter (Millipore). The sample concentration was measured by UV absorption at 280 nm using an extinction coefficient of 16 147 for the native protein (*20*). The concentration of protein in these experiments was about 1 mg/mL. The temperature dependence of the molar partial heat capacity (C_p) of SH3 was calculated from the DSC data and analyzed using Origin 5.0 (Microcal). C_p curves were fitted by a nonlinear least-squares method using a two-state

unfolding model as described previously (*20*). The enthalpy change of unfolding, ΔH_m, obtained from the fits was represented versus the unfolding temperature, T_m, for each pH* value. A temperature-independent heat capacity change of unfolding, ΔC_p, was estimated from this plot. This ΔC_p value, together with the ΔH_m and T_m values at each pH*, was used to calculate the global unfolding Gibbs energy change at 24.7 °C as described elsewhere (*20*).

Structure-Based Thermodynamic Analysis. The thermodynamic parameters associated with the folding/unfolding equilibrium of the SH3 domain were calculated from the crystallographic structure (PDB file 1shg) (*29*) using the structural parametrization of the energetics developed earlier (*30*−*35*).

The stability constants per residue were calculated according to the COREX algorithm (*16*, *17*, *36*). This algorithm generates a large ensemble of partially folded conformations and calculates the probability distribution of these states under a given set of conditions. For these calculations a total of 49 146 partially folded conformations were generated with the computer using the crystallographic structure (PDB file 1shg) as a template. The small size of the protein permitted the use of a very small window (four amino acids) without creating a computationally untractable number of states. The Gibbs energy of each state and its respective probability were calculated according to the structural parametrization of the energetics. For any particular residue j, the stability constant per residue, $k_{f,j}$, is calculated as the ratio of the summed probability, $P_{f,j,i}$, of all states in which residue j is folded, to the summed probability, $P_{nf,j,i}$, of all states in which that residue is not folded:

$$\kappa_{f,j} = \frac{\sum_i P_{f,j,i}}{\sum_i P_{nf,j,i}} \qquad (2)$$

It has previously been shown, through the analysis of various protein structures, that hydrogen exchange protection factors can be obtained from the stability constants per residue (*16*−*18*, *36*). The protection factor of residue j, PF_j, can be expressed in terms of probabilities:

$$PF_j = \frac{\sum_i P_{f,j,i} - \sum_i P^{ex}_{f,j,i}}{\sum_i P_{nf,j,i} + \sum_i P^{ex}_{f,j,i}} \qquad (3)$$

where the correction term $\sum_i P^{ex}_{f,j,i}$ is the sum of the probabilities of all states in which residue j is folded, yet exchange competent. The competence for exchange of residue j in a particular state i, is evaluated according to the exposition of the amide group to the solvent (*16*). Accessible surface area (ASA) calculations based on the method of Lee and Richards (*37*) are implemented within the COREX algorithm.

RESULTS AND DISCUSSION

Hydrogen Exchange Kinetics. The amide hydrogen−deuterium exchange for more than half of the α-spectrin SH3 residues can be followed under the experimental conditions used in this paper. In all cases the exchange shows first-order kinetics and allows an accurate determination of the exchange rate constants, k_{ex} (Figure 1). The experimental protection factors per residue are shown in Figure 2 (lower panels in each plot). Values are relatively low under our conditions and strongly dependent on pH*. Protected residues are grouped mainly in six regions of the protein sequence, corresponding to different elements of secondary structure: (a) residues 8−16, which correspond to the first β-strand (β1) and the first arm (β2) of the RT loop; (b) residues 22−26, corresponding to the second arm (β3) of the RT loop; (c) residues 30−34, corresponding to the β4 strand; (d) residues 41−46 forming the β5 strand; (e) residues 49−53 forming the β6 strand; (f) residues 55−61, corresponding to the short 3_{10} helix and the C-terminal (β7) strand. In general, residues located in the loops connecting secondary structures do not show measurable protection. An exception to this is Gly28, which is part of a diverging β-turn, separating the β3 and β4 strands and whose NH group forms a hydrogen bond with the C═O group of Ala11. Other

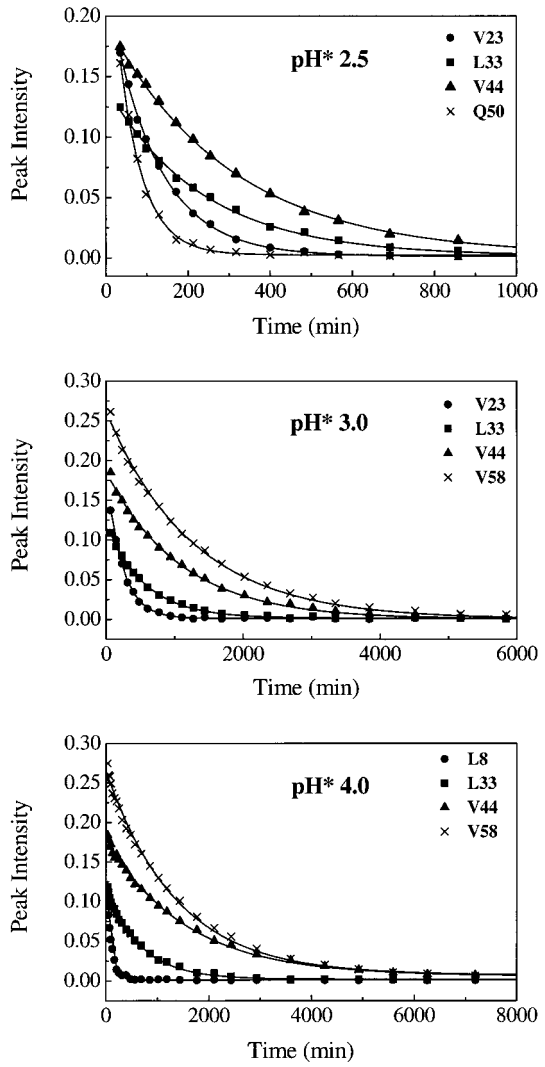

FIGURE 1: Amide hydrogen−deuterium exchange kinetics for several residues of α-spectrin SH3 at pH* 2.5, 3.0, and 4.0 and 24.7 °C. Each plot represents the dependence of the COSY NH−C_αH cross-peak intensity of some selected residues with the time of exchange at each pH* value. Symbols correspond to the experimental data. Solid lines are the best fits to a single-exponential decay function, from which the exchange rate constants have been derived.

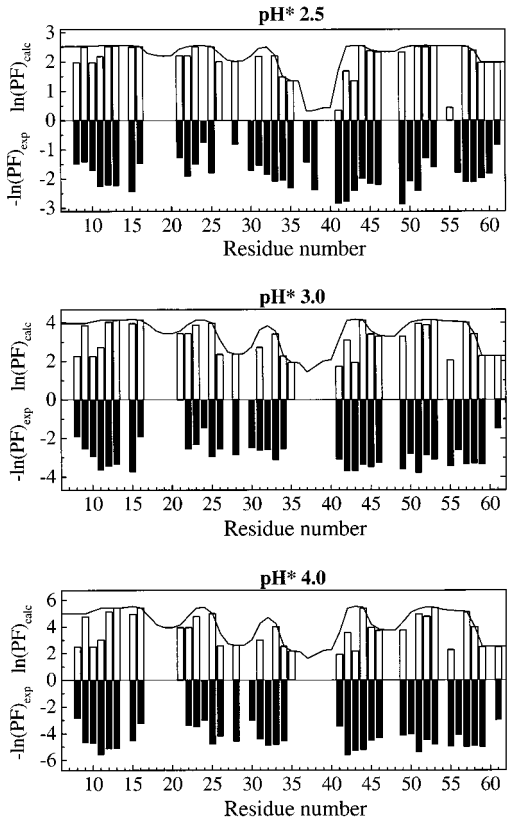

FIGURE 2: Pattern of protection factors (PF) per residue for α-spectrin SH3 at pH* values of 2.5, 3.0, and 4.0. Experimental values [$\ln(PF)_{exp}$] (solid bars) have been obtained from the exchange kinetics as described in Materials and Methods. Calculated values of the protection factors [$\ln(PF)_{calc}$] (open bars) and the stability constants per residue (solid lines) were calculated using the COREX algorithm from the crystal structure of the SH3 domain (see text). Upper and lower limits of each graph have been set to the values $\pm\Delta G_U/RT$, corresponding to the global unfolding of the protein, as determined by DSC, i.e., the expected value of ln(PF) for a residue that would exchange only upon the global unfolding of the protein.

exceptions are Thr37 and Asn38, which are located in the n-Src loop and show measurable protection at pH* 2.5. Two nonobservable Pro residues are at positions 20 and 54.

Differential Scanning Calorimetry. Since the exchange experiments are performed in D_2O, the global stability of the α-spectrin SH3 domain was measured by high-sensitivity differential scanning calorimetry (DSC) at different pH* values (Figure 3). As in the case of aqueous solutions, the heat capacity, C_p, curves obtained in deuterated buffers could be accounted very well by the two-state unfolding model *(20)*. This result indicates that within the transition region the conformational equilibrium of the SH3 domain is dominated by the native and unfolded states with no measurable influence of partially folded intermediates. The results of these experiments are summarized in Table 1 and Figure 4A. The enthalpy change of unfolding is dependent on the unfolding temperature as observed for this and other proteins in aqueous solution. At the reference temperature of 60 °C the enthalpy of unfolding ($\Delta H(60)$) was equal to 189 kJ/mol and the heat capacity change (ΔC_p) was equal to 3.9 kJ/(K·mol). These values are slightly higher from those obtained for the same protein in aqueous solution ($\Delta H(60) = 180$ kJ/mol and $\Delta C_p = 3.5$ kJ/(K·mol) (*20*)). Figure 4B shows the pD dependence of the Gibbs energy change of

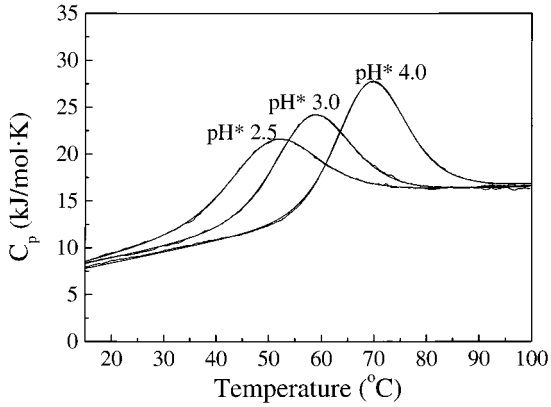

FIGURE 3: DSC thermograms of α-spectrin SH3 in deuterium oxide buffers at the three pH* values of the hydrogen exchange experiments. Experimental curves correspond to the partial molar heat capacity, C_p, of the protein. Best fits using a two-state unfolding model are shown practically superimposed to the experimental data.

Table 1: Thermodynamic Parameters for the Unfolding of the SH3 Domain of α-Spectrin in Deuterium Oxide Obtained by Differential Scanning Calorimetry

pH*	ΔH_m (kJ/mol)	T_m	pH*	ΔH_m (kJ/mol)	T_m
4.5	227	70.9	2.75	167	52.6
4.0	219	68.7	2.5	150	49.6
3.5	211	64.8	2.25	129	45.3
3.25	193	60.2	2.0	119	42.4
3.0	183	57.8	1.0	114	41.4

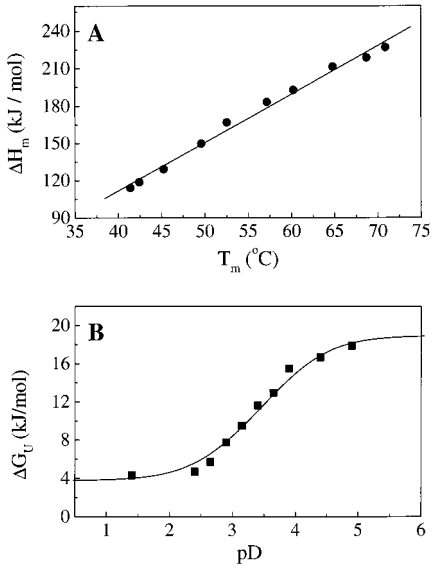

FIGURE 4: Panel A: Plot of the enthalpy change (ΔH_m) versus the temperature of unfolding (T_m) for α-spectrin SH3. Data represented with filled circles correspond to the experimental values obtained by DSC. The straight line is the least-squares fit to a linear dependence of the enthalpy change of unfolding versus temperature, from which a temperature-independent heat capacity change of unfolding, $\Delta C_p = 3.9 \pm 0.3$ kJ/(mol·K), has been estimated. Panel B: Dependence with pD of the Gibbs energy change for the global unfolding of SH3. Values at each pD (filled squares) were calculated from the DSC results. The solid line is the curve calculated using eq 4 (see Results). This calculation assumes that four carboxylic groups have anomalous pK_a's as discussed in the text.

global unfolding, ΔG_U, calculated from the DSC results at 25 °C. In this plot, the pH* values were transformed into pD values by adding 0.4 pH unit to the pH meter readings. It is clear that ΔG_U exhibits a sigmoidal dependence on pD

with a midpoint near pD 3.4. At pD 1.4 the stability of the protein is minimal and exhibits a ΔG_U of 4.3 kJ/mol. At pD 4.9 ΔG_U reaches a value of 17.9 kJ/mol. The slope of the curve indicates that at the midpoint of the pD curve (pD 3.4) an average of 1.2 protons becomes associated to the protein upon unfolding.

Global and Local Unfolding. The Gibbs energies corresponding to the global unfolding of the protein were 7.7, 11.6, and 16.7 kJ/mol at pH* 2.5, 3.0, and 4.0 respectively, at the same temperature in which the hydrogen exchange experiments were performed. The errors estimated for the global unfolding Gibbs energy changes determined from the DSC results are no larger than ±0.5 kJ/mol. Gibbs energy values per residue were also calculated from the hydrogen exchange data (eq 1) at the three pH* values considered in this work. The apparent Gibbs energies obtained from the experimental exchange data of practically all residues in the SH3 domain were consistently lower than the Gibbs energy change of global unfolding (see Figure 2). The only possible exceptions to this behavior were W41, W42, and R49 which at pH* 2.5 exhibit Gibbs energies of 7.05, 6.85, and 7.09 kJ/mol, respectively, and are within 1 kJ/mol of the global unfolding Gibbs energy. For all remaining residues, the individual Gibbs energies were lower than the global Gibbs energy by 1.6 kJ/mol or more. At pH* 3.0 and 4.0 the apparent Gibbs energies obtained from the exchange data were at least 2.0 kJ/mol lower than the global Gibbs energy. These results indicate that, under the experimental conditions considered in this paper, the amide exchange of essentially all residues in the domain occurs primarily via either local or subglobal unfolding reactions; i.e., none of the residues requires the complete unfolding of the protein in order to exchange its amide hydrogen with the solvent. In addition, there are no residues exhibiting superprotection, indicating that even residues in the most stable core of the protein become exposed by local unfolding and that no residual protection remains in the denatured state.

Analysis of the pH Dependence of the Gibbs Energy. From a general thermodynamic standpoint, the pH or pD dependence of the Gibbs energy change of an unfolding process, ΔG_U, can be expressed by the equation:

$$\Delta G_U = \Delta G_U^o - RT\sum_i \ln\left[\frac{1 + 10^{pK_{a,i} - pH}}{1 + 10^{pK_{a,i}^0 - pH}}\right] \qquad (4)$$

where ΔG_U^o is the Gibbs energy change at the reference pH, $pK_{a,i}$ is the pK of a group i in the unfolded state, and $pK_{a,i}^0$ is the pK_a of that group in the native state. As shown above, ΔG_U shows the characteristic sigmoidal dependence associated with a reaction coupled to a protonation reaction. For the thermodynamic analysis, the pH* values were transformed into pD values by adding 0.4 pH unit to the pH meter readings. Accordingly, in the pD scale the midpoint of the curve is centered at about pD 3.4. Even though the slope of the curve at the midpoint is consistent with the uptake of an average of 1.2 protons upon unfolding, several carboxylic groups might be contributing. Analysis of the crystallographic structure reveals the existence of four carboxylic groups, Glu7, Glu17, Glu22, and Asp40 which are substantially buried from the solvent or participate in the formation of salt bridges. These groups are expected to exhibit anomalous pK_a's and be the most likely contributors to the observed protonation effects. Application of the Tanford−Kirkwood algorithm (*38*) (García-Moreno, personal communication) to the crystallographic structure (PDB file 1shg) yielded pK_a's of 3.95, 2.48, 4.00, and 3.13 for those groups. Since in D_2O the pK_a's of the free groups are 4.15 for Glu and 3.75 for Asp, it seems that Glu17 and Asp 40 are the groups expected to have the most anomalous pK_a's and be the main contributors to the pH or pD dependence of the SH3 domain stability. In fact, these values account well for the experimental pD dependence of ΔG_U (Figure 4B). A nonlinear least-squares fit of the experimental data to four carboxylic groups did not change the pK_a values significantly and converged to pK_a's of 3.95, 2.48, 4.0, and 3.11, respectively. The intrinsic stability of the SH3 domain prior to the protonation of the carboxylic groups (ΔG_U^o) was found to be equal to 18.9 kJ/mol. The values for ΔG_U at 25 °C in D_2O buffers are in general slightly higher (from 0 to 2.4 kJ/mol depending on the pH/pH* values) than those obtained in aqueous solution (*20*). This indicates that there is a small increase in the stability of the SH3 domain produced by the D_2O/H_2O solvent exchange. This increase has been observed previously (*39*), although with some proteins a stability decrease in D_2O solutions has been reported (*40*).

Structure-Based Thermodynamic Analysis. The structure of the SH3 domain of α-spectrin has been solved crystallographically at 1.8 Å resolution (PDB file 1shg) (*29*). This structure was used to perform structure-based thermodynamic calculations using the structural parametrization of the energetics described before (*30*−*35*).

(A) Heat Capacity Change. The primary contributions to the heat capacity change upon protein unfolding arise as a result of the exposure to solvent of nonpolar and polar groups that were buried in the native state. For the SH3 domain of α-spectrin 3074 Å^2 of nonpolar, 1922 Å^2 of polar, and 110 Å of hydroxy surface area become exposed to the solvent upon unfolding. These changes in accessibility yield a ΔC_p of 3.77 kJ/(K·mol), which is very close to the experimental value of 3.9 kJ/(K·mol) obtained in this work and the value of 3.4 kJ/(K·mol) obtained previously in aqueous solution (*20*). Additional contributions such as those associated with the protonation of carboxylic groups contribute very little [about 0.15 kJ/(K·mol)].

(B) Enthalpy Change. The enthalpy change upon unfolding is dominated by two terms: a positive contribution due to the disruption of internal interactions (van der Waals, hydrogen bonds, etc.) and a negative term resulting from the solvation of groups that are buried in the native state (*33*). At 60 °C, the enthalpy change for unfolding of the SH3 domain predicted by the structural parametrization is 186 kJ/mol, which compares very well with the value of 180 kJ/mol obtained experimentally in H_2O and the value of 189 kcal/mol obtained here in D_2O.

The SH3 domain of α-spectrin has a packing density slightly higher than that of an average globular protein. For the SH3 domain of α-spectrin the average number of noncovalently bonded atoms within a distance of 3 Å is 4.6 compared to an average number of 4.4−4.5 for other proteins. This packing density is reflected in a higher magnitude of the enthalpy change as discussed before (*33*). Due to the atomic composition of this protein, these closely

packed atoms tend to be less polar than average, increasing the relative contributions of nonpolar van der Waals interactions to the enthalpy change.

(C) Entropy Change. The entropy change upon unfolding consists mainly of two opposing contributions, the conformational entropy increase of backbone and side chains and the negative change due to the solvation of groups that are buried from the solvent in the native state. The conformational entropy change amounts to 1.35 kJ/(K·mol) and the solvation entropy to −1.23 kJ/(K·mol), yielding a combined total of 0.12 kJ/(K·mol) at 25 °C. Together with the enthalpy change, the structural parametrization predicts a Gibbs energy of stabilization of 19.2 kJ/mol at 25 °C, in excellent agreement with the experimental value of 18.9 kJ/mol obtained from DSC.

The above results indicate that the structural parametrization of the energetics accounts accurately for the energetics of stabilization of the SH3 domain of α-spectrin and that the partitioning of the energetics into its enthalpic and entropic components is captured correctly.

Structure-Based Calculation of Hydrogen Exchange Protection Factors. A statistical thermodynamic formalism aimed at estimating stability constants at the residue level has been developed earlier (*16, 17, 36*). The stability constants per residue map the protein molecule in terms of the structural stability of different regions. Protein residues with a high probability of being in the native conformation are characterized by high stability constants while residues that are most likely to be unstructured have low stability constants. For the SH3 domain, the residue stability constants per residue calculated according to the COREX algorithm (*16, 17, 36*) are shown in Figure 2, together with the calculated values for the hydrogen exchange protection factors. These are compared with the experimentally determined values. As seen in the figure, the COREX algorithm predicts well the pattern of experimental protection factors. The standard deviation between experimental and calculated protection factors for those residues that exhibit protection is 4.6, 3.3, and 2.5 kJ/mol for the experiments at pH* 4.0, 3.0, and 2.5, respectively. These values are within the range obtained previously for other structure-based Δ*G* calculations (*16, 18, 35*). The residues with the largest errors appear to be randomly distributed within the SH3 structure and not to be concentrated within any particular structural region or secondary structural motif of the SH3 domain. Only one residue (Gln50) is mispredicted by more than 5 kJ/mol at the three pHs studied. Four other residues (Arg21, Ile30, Thr32, and Ala56) are mispredicted by more than 5.5 kJ/mol at pH 4 and 3 but predicted within 4 kJ/mol at pH 2.5. The agreement in the pattern and amplitude between predicted and experimental protection factors indicates that the ensemble of partially folded states predicted to be populated under native conditions is consistent with the one observed through the NMR-detected hydrogen exchange experiments. The differences between the calculated protection factors and the stability constants per residue that can be observed for some residues (Figure 2) are due to the probability that these particular residues be located in a folded region that becomes exposed to solvent upon the unfolding of a complementary region.

Structural Distribution of the Energetics of Stability. The pattern of hydrogen exchange protection reflects the statistical nature of the native state and the existence of an ensemble of conformations. If, under native conditions, only two states were accessible to the protein, the protection factors of all residues that show protection would be identical. This is certainly not the case for the SH3 domain or any other protein that has been measured by this technique, indicating that under native conditions proteins are characterized by the existence of multiple independent local unfolding events that give rise to a large number of conformational states. For some proteins, a certain number of residues exhibit the phenomenon of superprotection (see, for example, ref *41*). Usually, these residues are located either in highly stable protein cores or in regions that exhibit residual structure under denaturing conditions. This has been observed to be the case for the src SH3 domain at pH 6 (*42*). In the case of the SH3 domain of α-spectrin at acid pH this phenomenon is not observed since all residues have apparent Gibbs energies lower than the global unfolding Gibbs energy. Under the experimental conditions considered in this paper, essentially all amide groups in the domain undergo hydrogen−deuterium exchange via local unfolding reactions. The change from pH* 4.0 to pH* 2.5, with a strong decrease on global stability, does not appear to have a significant effect on the mechanism of exchange for the SH3 domain of α-spectrin. It can be noticed that, under the conditions of lower stability (pH* 2.5), the apparent Gibbs energy for some residues is approaching ΔG_U, indicating that the contribution of global unfolding to the exchange is increased. This is consistent with the effect of low denaturant concentrations observed for a number of proteins (see, for example, refs *8* and *43*). The pH dependence of the src SH3 domain might be different from that of the SH3 domain of α-spectrin due to a different proportion of acidic residues (four Glu and five Asp for α-spectrin versus four Glu, three Asp, and one His for src). In addition, the src SH3 domain appears to have a higher atomic packing density than the α-spectrin SH3 domain according to their high-resolution structures (PDB files 1shg and 1srl).

Figure 5 shows the structure of the SH3 domain color coded according to the structural stability of each residue. These results indicate that the most stable region of the SH3 domain is defined by the central portions of the β-strands—in particular the hairpin formed by the β5 and β6 strands at both sides of the distal loop, the short 3_{10} helix, and part of the long RT loop, whereas the loops connecting secondary structure exhibit lower stability. The peptide binding region, on the other hand, is composed of a highly stable region (residues 53−57) and a highly unstable region, the loop between residues 34−41 (n-Src loop).

Native State Ensemble of the SH3 Domain of α-Spectrin. In the calculations presented here, a total of 49 146 states were included. The majority of those states, however, have extremely high Gibbs energies and therefore negligible probabilities under native conditions. This observation reflects the basic cooperative nature of the folding process. To assess the structural characteristics of the native state ensemble, calculations were performed under conditions of maximal stability (ΔG_U = 19.2 kJ/mol) and the totality of the states was sorted in ascending Gibbs energy order. It was found that only 53 states out of the 49 146 had Gibbs energies lower than 21 kJ/mol (i.e., 0.13%). These states are illustrated in Figure 6. There were 43 states with lower Gibbs

FIGURE 5: Structure of the SH3 domain of α-spectrin color coded according to the magnitude of the stability constants per residue. In this figure blue denotes the most stable regions of the protein and the areas colored red the least stable regions. The stability constants were calculated with the COREX algorithm (*16, 17, 36*), and the figure was made using the program MOLSCRIPT (*45*).

energies and correspondingly higher probabilities than those of the unfolded state under native conditions. As shown in the figure, these states are created by the independent unfolding of small regions scattered throughout the entire domain. In fact, none of those states has more than eight residues in an unfolded conformation. Collectively, these local unfolding events are capable of exposing to solvent all amide groups in the protein even in the absence of global unfolding. These results account for the observation that the apparent Gibbs energy obtained for hydrogen exchange is lower than the Gibbs energy for global unfolding. In fact, at pH* 4 the Gibbs energies for exchange of even the most protected amides are close to 3 kJ/mol lower than the global Gibbs energy for unfolding, in agreement with the results shown in the figure.

Under native conditions, the dominant equilibrium is not the equilibrium between the native and unfolded states but the equilibrium between a large number of states exhibiting local independent "fluctuations" or "local unfolding" events that result in the loss of native state interactions at specific locations within the protein structure. An illustration of this scenario is the fact that under native conditions the probability of the "fully" folded state estimated from our calculations amounts to only ~72% whereas the remaining 28% is accounted mainly by the ensemble of states represented in Figure 6. Therefore, the native state ensemble is created by the occurrence of these local and independent unfolding events in all possible combinations and with probabilities dictated by their Gibbs energies. Since these events involve only a few residues, they are characterized by small enthalpies and small *m* values. As a result the Gibbs

FIGURE 6: Most probable conformations in the native ensemble of the SH3 domain of α-spectrin. Only the states with Gibbs energies lower than 21 kJ/mol have been included. The states were generated with the COREX algorithm (*16*) and account quantitatively for the pattern of hydrogen exchange protection factors. In this figure red represents native regions and yellow represents unfolded regions. The states represented have been ordered according to their Gibbs energies: first row, from 0 to 11.1 kJ/mol; second row, up to 13.8 kJ/mol; third row, up to 17.3 kJ/mol; fourth row, up to 18.9 kJ/mol; fifth row, up to 20.0 kJ/mol; sixth row, up to 21.0 kJ/mol. The Gibbs energy of the unfolded state (all yellow) is 19.2 kJ/mol.

energies of those states exhibit negligible temperature or denaturant concentration dependencies as observed experimentally (*8*, *11*, *13*, *44*). On the other hand, the completely unfolded state is characterized by large enthalpy and *m* values, and consequently the Gibbs energy for global unfolding exhibits considerable temperature and denaturant concentration dependencies. The net result of this behavior is that, as denaturation conditions are approached either thermally or chemically, the Gibbs energy for global unfolding decreases at a much faster rate and the equilibrium becomes dominated by the unfolded and native states. Thus, in the denaturation transition region the conformational equilibrium is well accounted for by the two-state model whereas under native conditions this model fails and the equilibrium needs to be considered in terms of statistical ensembles. The approach presented here provides a quantitative account of this behavior.

CONCLUSIONS

The NMR and calorimetric data presented here demonstrate the existence of multiple independent local unfolding events in the native state of the SH3 domain of α-spectrin. The most important consequence of these experiments is the redefinition of the concept of cooperativity in the native state. The observation that specific regions of a protein are able to undergo independent local folding/unfolding reactions indicates that under native conditions the scale of cooperative interactions is regional rather than global. Global cooperativity is only seen under denaturing conditions and appears to be the result of the characteristic dependencies of the Gibbs energies for different processes. The idea of an all-or-none behaving native state seems to be a product of the extrapolation of results obtained under denaturing conditions to native conditions. This extrapolation, however, does not provide an accurate representation of the properties of the native state ensemble.

ACKNOWLEDGMENT

We thank Dr. Luis Serrano for kindly providing the WT-SH3 plasmid and Dr. Bertrand García-Moreno for performing the pK_a calculations from structure and for many helpful discussions. We also thank Dr. Irene Luque for many helpful discussions. Finally, we thank the Scientific Instrumentation Center of the University of Granada for their technical support in the NMR experiments.

REFERENCES

1. Jeng, M.-F., and Englander, S. W. (1991) *J. Mol. Biol. 221*, 1045−1061.
2. Radford, S. E., Buck, M., Topping, K. D., Dobson, C. M., and Evans, P. A. (1992) *Proteins 14*, 237−248.
3. Loh, S. N., Prehoda, K. E., Wang, J., and Markley, J. L. (1993) *Biochemistry 32*, 11022−11028.
4. Kim, K.-S., and Woodward, C. (1993) *Biochemistry 32*, 9609−9613.
5. Woodward, C. (1993) *Trends Biochem. Sci. 18*, 359−360.
6. Clarke, J., and Fersht, A. R. (1996) *Folding Des. 1*, 243−254.
7. Swint-Kruse, L., and Robertson, A. D. (1996) *Biochemistry 35*, 171−180.
8. Bai, Y., Sosnick, T. R., Mayne, L., and Englander, S. W. (1995) *Science 269*, 192−197.
9. Jacobs, M. D., and Fox, R. O. (1994) *Proc. Natl. Acad. Sci. U.S.A. 91*, 449−453.
10. Morozova, L. A., Haynie, D. T., Arico-Muendel, C., Van Dael, H., and Dobson, C. M. (1995) *Nat. Struct. Biol. 2*, 871−875.
11. Bai, Y., and Englander, S. W. (1996) *Proteins 24*, 145−151.
12. Schulman, B. A., Redfield, C., Peng, Z., Dobson, C. M., and Kim, P. S. (1995) *J. Mol. Biol. 253*, 651−657.
13. Chamberlain, A. K., and Marqusee, S. (1998) *Biochemistry 37*, 1736−1742.
14. Hvidt, A., and Nielsen, S. O. (1966) *Adv. Protein Chem. 21*, 287−386.
15. Kim, K.-S., Fuchs, J. A., and Woodward, C. K. (1993) *Biochemistry 32*, 9600−9608.
16. Hilser, V. J., and Freire, E. (1996) *J. Mol. Biol. 262*, 756−772.
17. Hilser, V. J., and Freire, E. (1997) *Proteins 27*, 171−183.
18. Hilser, V. J., Dowdy, D., Oas, T. G., and Freire, E. (1998) *Proc. Natl. Acad. Sci. U.S.A. 95*, 9903−9908.
19. Kuriyan, J., and Cowburn, D. (1993) *Curr. Opin. Struct. Biol. 3*, 828−837.
20. Viguera, A. R., Martinez, J. C., Filimonov, V. V., Mateo, P. L., and Serrano, L. (1994) *Biochemistry 33*, 2142−2150.
21. Morton, C. J., and Campbell, I. D. (1994) *Curr. Biol. 4*, 615−617.
22. Pawson, T. (1995) *Nature 373*, 573−580.
23. Xu, W., Harrison, S. C., and Eck, M. J. (1997) *Nature 385*, 595−602.
24. Marion, D., and Wuthrich, K. (1983) *Biochem. Biophys. Res. Commun. 113*, 967−974.
25. Delaglio, F., Grzesiek, S., Vuister, G. W., Zhu, G., Pfeifer, J., and Bax, A. (1995) *J. Biomol. NMR 6*, 277−293.
26. Johnson, B. A., and Blevins, R. A. (1994) *J. Biomol. NMR 4*, 603−614.
27. Blanco, F., Ortiz, A. R., and Serrano, L. (1997) *J. Biomol. NMR 9*, 347−357.
28. Bai, Y., Milne, J. S., Mayne, L., and Englander, S. W. (1993) *Proteins 17*, 75−86.
29. Musacchio, A., Noble, M., Pauptit, R., Wierenga, R., and Saraste, M. (1992) *Nature 359*, 851−855.
30. Gomez, J., Hilser, J. V., Xie, D., and Freire, E. (1995) *Proteins: Struct., Funct., Genet. 22*, 404−412.
31. Gomez, J., and Freire, E. (1995) *J. Mol. Biol. 252*, 337−350.
32. D'Aquino, J. A., Gómez, J., Hilser, V. J., Lee, K. H., Amzel, L. M., and Freire, E. (1996) *Proteins 25*, 143−156.
33. Hilser, V. J., Gomez, J., and Freire, E. (1996) *Proteins 26*, 123−133.
34. Luque, I., Mayorga, O., and Freire, E. (1996) *Biochemistry 35*, 13681−13688.
35. Bardi, J. S., Luque, I., and Freire, E. (1997) *Biochemistry 36*, 6588−6596.
36. Hilser, V. J., Townsend, B. D., and Freire, E. (1997) *Biophys. Chem. 64*, 69−79.
37. Lee, B., and Richards, F. M. (1971) *J. Mol. Biol. 55*, 397−400.
38. García-Moreno, B. E. (1995) *Methods Enzymol. 259*, 512−538.
39. Swint-Kruse, L., and Robertson, A. D. (1995) *Biochemistry 34*, 4724−4732.
40. Makhatazde, G. I., Clore, G. M., and Gronenborn, A. M. (1995) *Nat. Struct. Biol. 2*, 852−855.
41. Bai, Y., Milne, J. S., Mayne, L., and Englander, S. W. (1994) *Proteins 20*, 4−14.
42. Grantcharova, V. P., and Baker, D. (1997) *Biochemistry 36*, 15685−15692.
43. Qian, H., Mayo, S. L., and Morton, A. (1994) *Biochemistry 33*, 8167−8171.
44. Chamberlain, A. K., Handel, T. M., and Marqusee, S. (1996) *Nat. Struct. Biol. 3*, 782−787.
45. Kraulis, P. J. (1991) *J. Appl. Crystallogr. 24*, 946−950.

BI990413G